Polymer 51 (2010) 4243–4248

Contents lists available at ScienceDirect

Polymer

journal homepage: www.elsevier.com/locate/polymer

Solution properties of amylose tris(*n*-butylcarbamate). Helical and global conformation in alcohols

Yuichi Sano [a], Ken Terao [a,*], Shota Arakawa [a], Masahiro Ohtoh [a], Shinichi Kitamura [b], Takashi Norisuye [a]

[a] Department of Macromolecular Science, Graduate School of Science, Osaka University, 1-1 Machikaneyama-cho, Toyonaka, Osaka 560-0043, Japan
[b] Graduate School of Life and Environmental Sciences, Osaka Prefecture University, Gakuen-cho, Nakaku, Sakai, Osaka 599-8531, Japan

ARTICLE INFO

Article history:
Received 2 February 2010
Received in revised form
9 June 2010
Accepted 25 June 2010
Available online 17 July 2010

Keywords:
Polysaccharide derivative
Hydrogen bond
Chain stiffness

ABSTRACT

Particle scattering functions $P(k)$, z-average radii of gyration $\langle S^2\rangle_z^{1/2}$, intrinsic viscosities $[\eta]$, infrared absorption (IR) spectra, and specific rotations have been determined by light and/or small-angle X-ray scattering, viscometry, IR, and polarimetry for narrow distribution samples of amylose tris(*n*-butylcarbamate) (ATBC) ranging in weight-average molecular weight from 1.7×10^4 to 1.7×10^6 in 2-propanol at 35 °C, 1-propanol at 40 (or 35) °C, 2-ethoxyethanol at 25 °C, and 2-butanol at 45 °C. The two propanols are found to attain the theta state at 35 °C. The number fraction f_{1698} of intramolecular hydrogen bonds between the C=O and NH groups of the ATBC chain is obtained from IR spectra, and the helix pitch h (or the contour length) per residue and the Kuhn segment length λ^{-1} are estimated to be 0.25–0.29 nm and 20–40 nm, respectively, from analyses of $P(k)$, $\langle S^2\rangle_z$, and $[\eta]$ data on the basis of the wormlike chain. The relationship among the three parameters (f_{1698}, h, and λ^{-1}) in the four alcohols and that among the previous estimates in tetrahydrofuran-methanol mixtures are explained in a unified manner by a two-state model, in which each chain consists of semiflexible (loosely helical) and rodlike (rigid helical) sequences. Namely, h increases when intramolecular hydrogen bonds are broken. This differs from the case of amylose tris(phenylcarbamate) for which the bulkiness of polar solvent molecules extends the helix of the polymer.

1. Introduction

Secondary structures of most biopolymers [1] and some foldamers [2,3] are stabilized by intramolecular hydrogen bonds (H-bonds), whose strength is often comparable to the H-bonding with solvent molecules, and therefore they are affected strongly by polymer–solvent interactions. Amylose tris(*n*-butylcarbamate) (ATBC, Fig. 1), first synthesized for use of chiral stationary phase in gas chromatography [4], is such a polymer, in that it has tightly-wounded rigid helical structure stabilized by intramolecular H-bonding between its C=O and NH groups in tetrahydrofuran (THF) [5]. In fact, the helix pitch h (or the contour length) per residue estimated on the basis of the wormlike chain [6] is 0.26 nm, a value much smaller than those (0.37–0.40 nm) of amylose triesters in the crystalline state [7], while the Kuhn segment length λ^{-1} (or more generally, the stiffness parameter in the helical wormlike chain [8,9]) is as large as 75 nm.

This rigid ATBC helix, whose possible 3D structure [5] is shown in Fig. 1, loosens as methanol (MeOH) is successively added to the THF solution, and its h and λ^{-1} finally reach 0.32 nm and 11 nm, respectively, in pure MeOH. These changes in the parameter set with increasing MeOH content accompany not only decreases in dimensional and hydrodynamic properties but also the breaking of intramolecular H-bonds as detected by the splitting amide I band (associated primarily with C=O stretching) in infrared absorption (IR) spectra [5]. The relationship among h, λ^{-1}, and the number fraction f_{1698} of intramolecularly H-bonded C=O groups in THF-MeOH mixtures is successfully explained by a two-state model, in which each chain consists of randomly distributed rigid helical and semiflexible (loosely helical) sequences.

Fig. 2 shows preliminary determined intrinsic viscosities $[\eta]$ for an ATBC sample (ATBC1700K) with a weight-average molecular weight of 1.67×10^6 in various alcohols and ethers; the line connects the data points that are displayed just in the order of increasing $[\eta]$. Interestingly, $[\eta]$ varying with the kind of alcohol covers a substantial range between THF and MeOH, indicating that a series of alcohols may be used as solvents to check the applicability of the two-state model to ATBC, as was done with THF-MeOH

* Corresponding author. Tel.: +81 6 6850 5459; fax: +81 6 6850 5461.
E-mail address: kterao@chem.sci.osaka-u.ac.jp (K. Terao).

0032-3861/$ – see front matter © 2010 Elsevier Ltd. All rights reserved.
doi:10.1016/j.polymer.2010.06.048

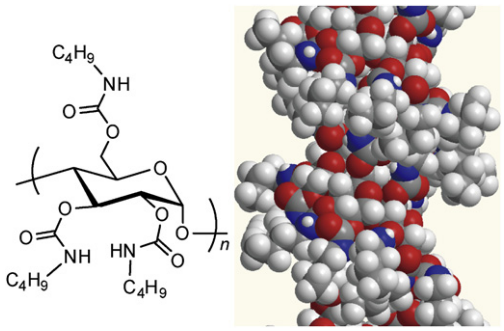

Fig. 1. Chemical structure of ATBC and possible helical structure [5] in THF.

mixtures. We note that those alcohols allow observation of the amide I band and hence the estimation of f_{1698}.

The present study was undertaken to deepening our understanding of solvent effects on the conformation of ATBC by determining h, λ^{-1}, and f_{1698} in 1-propanol (1PrOH) at 40 (or 35) °C, 2-propanol (2PrOH) at 35 °C, 2-ethoxyethanol (2EE) at 25 °C, and 2-butanol (2BuOH) at 45 °C from light and small-angle X-ray scattering, viscosity, IR, and optical rotation measurements. If intramolecular H-bonding plays an essential role in the ATBC conformation, the helix may be tightened and stiffened with increasing $[\eta]$ in harmony with the two-state model mentioned above. In contrast to such a decrease in h, however, it is also likely that the helix extends in a more bulky alcohol, thereby increasing $[\eta]$ (see Fig. 2). This conjecture is based on our previous finding [10,11] that in ester and ketone solvents, the helix of amylose tris(phenylcarbamate) (ATPC) measurably extends and becomes stiffer as the molar volume of the solvent increases. In the work reported below, we present scattering, viscosity, and spectroscopic data for ATBC samples and their analyses based on the wormlike chain and the two-state model.

2. Experimental

2.1. Samples and solvents

Ten fully substituted ATBC samples [5] (ATBC1700K, ATBC900K, ATBC700K, ATBC460K, ATBC250K, ATBC130K, ATBC110K, ATBC55K, ATBC53K, and ATBC17K) were used for this study. These samples had been prepared from enzymatically synthesized amylose [12] having narrow molecular weight distribution and no branching. Their weight-average molecular weights M_w ranged from 1.7×10^4 to 1.7×10^6 and their polydispersity indices were about 1.1 [5]. 2PrOH, 1PrOH, 2EE, and 2BuOH were purified by fractional distillation over granular calcium hydride.

2.2. Static light scattering (SLS)

SLS measurements were made for ATBC900K, ATBC700K, and ATBC250K in 1PrOH and 2PrOH, and for ATBC1700K in 2PrOH on a Fica-50 light scattering photometer with vertically polarized incident light of 436 or 546 nm wavelength (λ_0). The experimental details including the calibration of the photometer were described previously [10]. The specific refractive index increments $\partial n/\partial c$ at $\lambda_0 = 436$, 546, and 633 nm were determined for ATBC1700K in 2PrOH at 30, 35, and 40 °C and ATBC460K in 1PrOH at 30 and 40 °C. The $\partial n/\partial c$ values in 2PrOH at 35 °C were 0.112, 0.109, 0.108 cm^3g^{-1} at $\lambda_0 = 436$, 546, and 633 nm, respectively, while those in 1PrOH at 40 °C were 0.100, 0.097, 0.095 cm^3g^{-1} at $\lambda_0 = 436$, 546, and 633 nm, respectively. These values in either solvent did not differ more than 1% from those at the other temperatures for the corresponding λ_0.

The linear [13] and square-root [14] plots were used to extrapolate Kc/R_θ to $c = 0$ and $\theta = 0$, respectively; here, K is the optical constant, R_θ the reduced scattering intensity, c the polymer mass concentration, and θ the scattering angle. The second virial coefficients A_2 obtained for ATBC700K, ATBC900K, and ATBC1700K in 2PrOH are plotted against temperature T in Fig. 3a. They vanish at 35 °C, indicating that 2PrOH at 35 °C is a theta solvent for ATBC. Although this polymer in 1PrOH also attained the theta state at 35 °C as shown in Fig. 3b, we found the presence of a small amount of aggregates in its solutions at the theta point, and thus studied this polymer + solvent system at a little higher T of 40 °C, too.

2.3. Small-angle X-ray scattering (SAXS)

SAXS measurements were made for ATBC55K and ATBC17K in 2PrOH at 35 °C, 1PrOH at 35 °C, and 2EE at 25 °C and for ATBC53K in 2BuOH at 45 °C with an imaging plate detector at the BL40B2 Beamline in SPring-8. The camera length and λ_0 were chosen to be 1500 mm and 0.1 nm, respectively. To determine the z-average mean-square radius of gyration $\langle S^2 \rangle_z$ and the particle scattering function $P(k)$ (k denotes the magnitude of the scattering vector), four solutions of different concentrations and the solvent were measured, and the resultant intensity data were analyzed by use of the square-root plot [14] (See Ref. [10] for more experimental details).

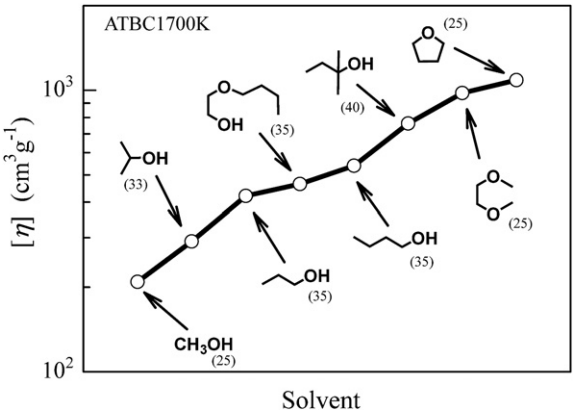

Fig. 2. Intrinsic viscosities $[\eta]$ for ATBC1700K in indicated solvents at temperatures (°C) shown in the parentheses.

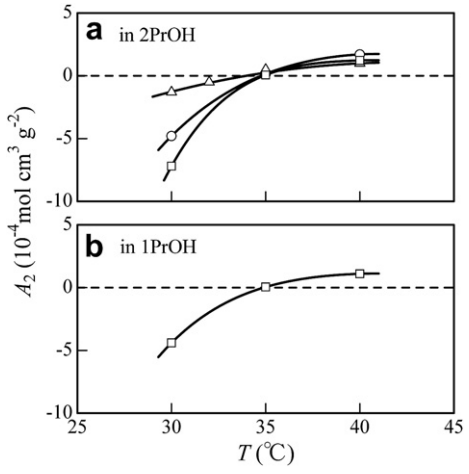

Fig. 3. Temperature dependence of A_2 for ATBC700K (circles), ATBC900K (squares), and ATBC1700K (triangles) in 2PrOH (a) and in 1PrOH (b).

2.4. Viscometry

Solvent and solution viscosities for ATBC900K, ATBC700K, ATBC250K, ATBC130K, ATBC110K, and ATBC17K in 2PrOH at 35 °C, 1PrOH at 40 °C, 2EE at 25 °C, and 2BuOH at 45 °C, and for ATBC55K in 2PrOH at 35 °C were measured using an Ubbelohde type viscometer. The relative viscosity was evaluated by taking into account the difference between the solution and solvent densities. The Huggins constant k' ranged from 0.4 to 0.9 in 2PrOH, from 0.4 to 0.7 in 1PrOH, from 0.4 to 1.3 in 2EE, and from 0.3 to 0.5 in 2BuOH.

2.5. Infrared absorption (IR) and optical rotation (OR)

IR and OR data were taken for ATBC samples (ATBC900K, ATBC700K, or ATBC460K) in 2PrOH at 35 °C, 1PrOH at 35 and 40 °C, 2EE at 25 °C, and 2BuOH at 45 °C on a J720WO spectropolarimeter (JASCO) with a 10-cm cell and on an FT/IR-4200 (JASCO) with a solution cell made of CaF_2 and having 0.05-mm path length. The polymer mass concentration was adjusted to 0.5–1.5 $\times$ 10^{-2} g cm^{-3}.

3. Results and discussion

3.1. Molecular weight and dimensional properties

The angular dependence of $P(k)^{-1/2}$ evaluated from SLS and SAXS intensities is illustrated in Fig. 4. The values of $\langle S^2\rangle_z^{1/2}$ determined from the initial slopes (the dashed lines) of the indicated solid lines are summarized in Tables 1 and 2, along with those of M_w. The former table includes $\langle S^2\rangle_z^{1/2}$ data in 2PrOH and 1PrOH at different temperatures. It can be seen in this table that the values of $\langle S^2\rangle_z^{1/2}$ for the respective samples in either 2PrOH or 1PrOH at 35 and 40 °C are very close to each other. We may therefore use the SAXS data of $\langle S^2\rangle_z^{1/2}$ in 1PrOH at 35 °C as those at 40 °C in our analysis of the M_w-dependence of $\langle S^2\rangle_z^{1/2}$. Another point to note is that the values of M_w in the propanols are in good agreement with those in THF and MeOH [5] (not presented here).

The Holtzer plots [15] [$kP(k)$ vs k] illustrated in Fig. 5 were analyzed on the basis of the Nakamura-Norisuye theory [16] for the cylindrical wormlike chain, which is characterized by three parameters, L (the contour length), λ^{-1}, and d (the cylinder diameter). The first parameter is related to the molar mass M of the chain by

$$L = M/M_L \tag{1}$$

where M_L denotes the molar mass per unit contour length. The two parameters, M_L and d, were unequivocally determined by curve fitting in the k range between 0.5 and 2.5 nm^{-1} for ATBC55K and ATBC53K and that between 1 and 2.5 nm^{-1} for ATBC17K; we note that this was possible because the theoretical $P(k)$ in such a k range exhibits the rod-limiting behavior as indicated by dashed lines for $\lambda^{-1} = \infty$. The dashed curves for ATBC55K in 2PrOH and 1PrOH deviate appreciably from the plotted points for $k < 0.5$ nm^{-1}, allowing the third parameter λ^{-1} to be estimated by utilization of the deviations. The solid curves for these solvents represent the theoretical values for the wormlike cylinders with the parameters listed in Table 3. On the other hand, in 2EE and 2BuOH, the data points are closely fitted by the dashed curves for the straight cylinders, indicating that the λ^{-1} values in the two solvents should be larger than those in the propanols and cannot be determined from the present $P(k)$ data alone. The solid curves for 2EE and 2BuOH are indeed indistinguishable from these dashed lines for the rod limit, where for their calculation we have used the λ^{-1} values obtained from $[\eta]$ (see below).

Fig. 6 displays the molecular weight dependence of $\langle S^2\rangle_z^{1/2}$ in 2PrOH at 35 °C and in 1PrOH at 40 °C (or 35 °C). The slopes of the

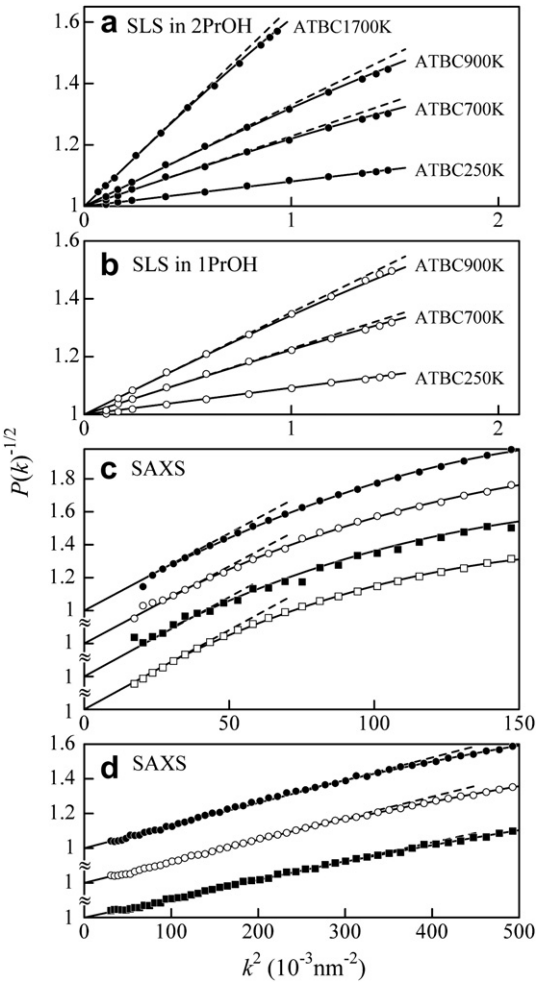

Fig. 4. Berry plots constructed from SLS (panels a and b) and SAXS data (panels c and d) for ATBC samples in 2PrOH (filled circles) at 35 °C, in 1PrOH (open circles) at 40 °C (35 °C for SAXS), in 2EE (filled squares) at 25 °C, in 2BuOH (open squares) at 45 °C. (c), For ATBC55K in 2PrOH, 1PrOH, and 2EE and for ATBC53K in 2BuOH from top to bottom; (d), for ATBC17K (symbols are the same as those used in panel c).

curves gradually decrease from 0.85 to 0.55 with increasing M_w, as typically observed for polymers modeled by the wormlike chain. The unperturbed mean-square radius of gyration $\langle S^2\rangle$ for this chain is given by [17]

$$\left\langle S^2\right\rangle = \frac{M}{6\lambda M_L} - \frac{1}{4\lambda^2} + \frac{M_L}{4\lambda^3 M} - \frac{M_L^2}{8\lambda^4 M^2}\left[1 - \exp\left(-\frac{2\lambda M}{M_L}\right)\right] \tag{2}$$

If the effect of chain diameter d is considered, a term $d^2/8$ adds to the right-hand side of this equation [18], but its contribution calculated with the d of 1.3 nm from $P(k)$ is 0.21 nm^2, a value negligible (~2.7%) compared to the experimental $\langle S^2\rangle_z$ (~7.7 nm^2) for the lowest M_w sample. The two parameters (M_L and λ^{-1}) determined by the curve fitting procedure agree with those from $P(k)$ (Table 3).

3.2. Intrinsic viscosity

The molecular weight dependence of $[\eta]$ illustrated in Fig. 7 was analyzed by using the Yamakawa-Fujii-Yoshizaki theory [8,19,20] for unperturbed wormlike cylinders. Although SAXS intensity data suggested that 2EE at 25 °C and 2BuOH at 45 °C are good (or marginal) and poor solvents, respectively, for ATBC, excluded-

Table 1
Results from light scattering measurements on ATBC samples in 2-propanol (2PrOH) and 1-propanol (1PrOH).

Sample	in 2PrOH at 35 °C		in 1PrOH at 40 °C	
	$M_w/10^4$	$\langle S^2\rangle_z^{1/2}$ (nm)	$M_w/10^4$	$\langle S^2\rangle_z^{1/2}$ (nm)
ATBC1700K	161	64[d]		
		63		
		57[b]		
		56[a]		
ATBC900K	88.9	45[d]	92.6	46
		45		45[c]
		40[a]		39[a]
ATBC700K	69.4	39[d]	69.9	37
		37		
		34[a]		
ATBC250K	25.5	22.0	25.3	23.5
				23.9[c]

[a] 30 °C.
[b] 32 °C.
[c] 35 °C.
[d] 40 °C.

volume effects in the two solvents were ignored in the M_w range investigated; this may be rationalized by the fact that the chain stiffness is much higher in these solvents than in MeOH, a good solvent (see Table 4) in which the effects were negligibly small [5]. The solid curves in Fig. 7 show that the theoretical values calculated with the parameters in Table 3 fairly well fit the experimental data; we assumed M_L to equal the value from $P(k)$. The estimated d values (~3 nm) are close to those reported previously for ATBC in THF-MeOH mixtures [5].

The values of λ^{-1} evaluated are in substantial agreement with those obtained from $P(k)$ and $\langle S^2\rangle_z$, indicating that the three properties of ATBC in the four alcohols are consistently explained by the current theories for the wormlike chain. However, the d values from $[\eta]$ are much larger than those from $P(k)$ as was the case with ATBC in THF and MeOH [5] and ATPC in various solvents [10,11]. This is because the former is the hydrodynamic thickness which is affected by H-bonding solvent molecules while the latter reflects the electron density profile (including solvent molecules) around the chain contour of ATBC in solution.

The mean of λ^{-1} and that of h calculated from M_0/M_L (the molar mass per residue $M_0 = 459.5$) are presented in Table 4, along with those in THF and MeOH. Importantly, h tends to decrease as λ^{-1} increases.

3.3. Intramolecular H-bonding and optical rotation

Fig. 8 shows IR spectra around the amide I band (1650–1800 cm^{-1}) for ATBC460K in the four alcohols, 2PrOH, 1PrOH, 2EE, and 2BuOH, and our previous data [5] in THF and MeOH. The features of the solvent-dependent peaks resemble those previously observed for ATBC in THF-MeOH mixtures, and as was done for the mixed solvent system, the peaks were each separated into three; we ignored the difference in measured T among the solvents because IR spectra were insensitive to T in the range concerned. The two peaks at 1698 cm^{-1} (intramolecular H-bonding between C=O and NH groups) and 1718 cm^{-1} (intermolecular H-bonding between a C=O group of the polymer and the solvent) were found at the same positions as those in THF and MeOH, respectively, while the peak wavenumber for the "free" C=O group varying between 1724 and 1730 cm^{-1} in the four alcohols is slightly smaller than that in THF (1737 cm^{-1}) but close to the theoretical value 1728 cm^{-1} evaluated for methyl methylcarbamate [5] using the DFT calculation (Gaussian 03). The slightly smaller wavenumbers in the four alcohols than in THF are possibly due to solvent characteristics such as the dielectric constant. In any event, since the total area of the three peaks is substantially independent of the kind of solvent, the area fraction f_{1698} of the peak at 1698 cm^{-1} may be regarded as the number fraction of intramolecularly H-bonded C=O groups in each chain.

Table 2
Results from SAXS measurements on ATBC samples in 2PrOH at 35 °C, 1PrOH at 35 °C, 2-ethoxyethanol (2EE) at 25 °C, and 2-butanol (2BuOH) at 45 °C.

Sample	$M_w/10^4$ [a]	$\langle S^2\rangle_z^{1/2}$ (nm)			
		in 2PrOH	in 1PrOH	in 2EE	in 2BuOH
ATBC55K	5.45	7.5	7.5	7.6	
ATBC53K	5.30				7.6
ATBC17K	1.66	2.80	2.75	2.55	

[a] Ref [5].

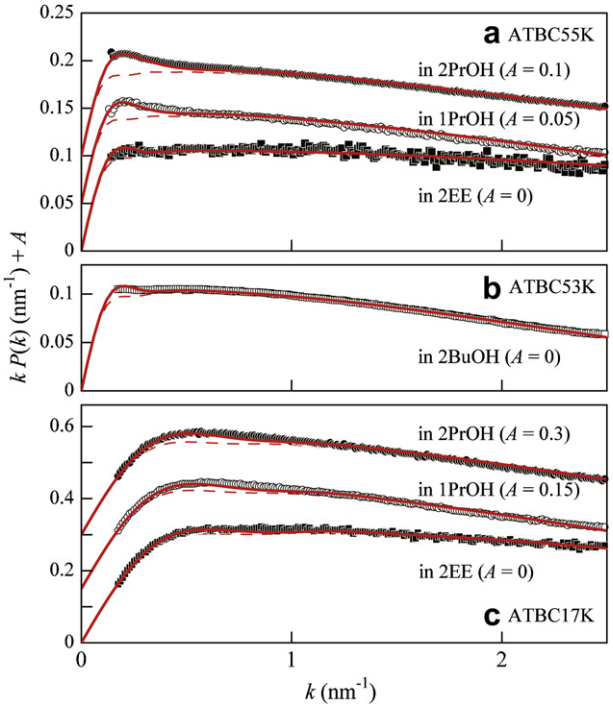

Fig. 5. Holtzer plots for indicated ATBC samples in 2PrOH (filled circles) at 35 °C, in 1PrOH (open circles) at 35 °C, in 2EE (filled squares) at 25 °C, and in 2BuOH (open squares) at 45 °C. The ordinate values are shifted by A for clarity. Solid and dashed curves represent theoretical values for the unperturbed wormlike cylinder with the parameters in Table 3 and those in the rod limit ($\lambda^{-1} = \infty$), respectively.

Table 3
Wormlike chain parameters for ATBC in 2PrOH at 35 °C, 1PrOH at 40 °C, 2EE at 25 °C, and 2BuOH at 45 °C.

Method	M_L (nm^{-1})	λ^{-1} (nm)	d (nm)
in 2PrOH at 35 °C			
$P(k)$	1590 ± 40	19 ± 2	1.3 ± 0.1
$\langle S^2\rangle_z$	1600 ± 50	22 ± 2	–
$[\eta]$	1590[a]	18 ± 2	3.2 ± 0.3
in 1PrOH at 40 °C			
$P(k)$	1680 ± 40	26 ± 3	1.3 ± 0.1
$\langle S^2\rangle_z$	1630 ± 50	25 ± 2	–
$[\eta]$	1680[a]	24 ± 3	2.7 ± 0.3
in 2EE at 25 °C			
$P(k)$	1840 ± 50	38[a]	0.8 ± 0.1
$[\eta]$	1840[a]	38 ± 4	3.0 ± 0.3
in 2BuOH at 45 °C			
$P(k)$	1830 ± 50	40[a]	1.3 ± 0.1
$[\eta]$	1830[a]	40 ± 5	3.0 ± 0.3

[a] Assumed values.

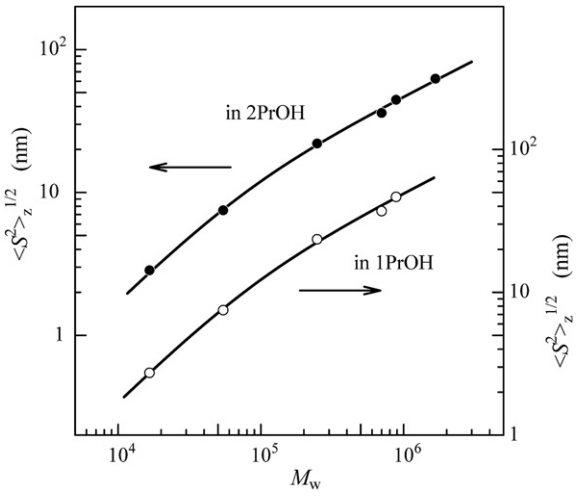

Fig. 6. Molecular weight dependence of $\langle S^2\rangle_z^{1/2}$ for ATBC in 2PrOH (filled circles) at 35 °C and in 1PrOH (open circles) at 40 °C (35 °C for the two lowest M_w samples). Curves, theoretical values calculated for the wormlike chains with the parameters in Table 3.

Fig. 9a shows specific optical rotations $[\alpha]_{280}$ at $\lambda_0 = 280$ nm plotted against f_{1698} for ATBC in the four alcohols and THF-MeOH mixtures. The linear decrease in $[\alpha]_{280}$ with an increase in f_{1698} suggests that the number fraction of H-bonded C=O groups reflects such a local conformational property as the helicity of ATBC as was previously found to be the case in THF-MeOH mixtures. The order of increasing f_{1698} (MeOH < 2PrOH < 1PrOH < 2EE ~ 2BuOH < THF) almost coincides with that of lowering dielectric constant (MeOH > 1PrOH ~ 2PrOH > 2EE ~ 2BuOH > THF) as may be expected.

3.4. Analysis in terms of a two-state model

In our previous study [5], the relationship among h, λ^{-1}, and f_{1698} for ATBC in THF-MeOH mixtures was interpreted by a two-state model, in which a given monomeric unit is in either of the states F and R and the polymer chain consists of randomly distributed

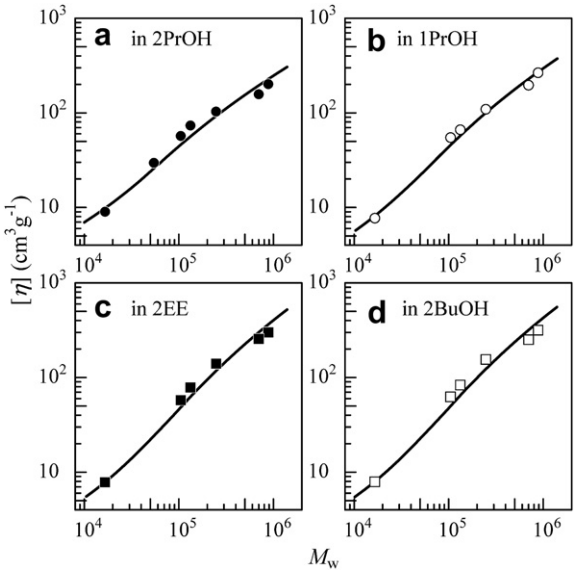

Fig. 7. Molecular weight dependence of $[\eta]$ for ATBC in 2PrOH at 35 °C (a), in 1PrOH at 40 °C (b), in 2EE at 25 °C (c), and in 2BuOH at 45 °C (d). Curves, theoretical values calculated for the wormlike chains with the parameters in Table 3.

Table 4
Values of the helix pitch per residue h and the Kuhn segment length λ^{-1} for ATBC in various solvents.

Solvent	T (°C)	h (nm)	λ^{-1} (nm)
MeOH[a]	25	0.32 ± 0.01	11 ± 2
2PrOH	35	0.29 ± 0.01	20 ± 2
1PrOH	40	0.28 ± 0.01	25 ± 2
2EE	25	0.25 ± 0.01	38 ± 4
2BuOH	45	0.25 ± 0.01	40 ± 5
THF[a]	25	0.26 ± 0.01	75 ± 5

[a] Ref [5].

semiflexible (F) and rodlike (R) sequences. We denote the Kuhn length and the contour length per residue of the pure R chain by λ_R^{-1} and h_R, respectively, and the corresponding parameters for the pure F chain by λ_F^{-1} and h_F. Then we can express h and λ^{-1} leading to eq. (2) as [21]

$$h = F_R h_R + (1 - F_R) h_F \tag{3}$$

$$\lambda h = F_R \lambda_R h_R + (1 - F_R) \lambda_F h_F \tag{4}$$

where F_R is the number fraction of the R monomer (=f_{1698}/f_R with f_R the value of f_{1698} for the homopolymer R). With this proportionality between F_R and f_{1698} in mind, we have illustrated the f_{1698}-dependence of h and λh for ATBC in the four alcohols and THF-MeOH mixtures in panels b and c of Fig. 9. The data points in either panel are fitted by a straight line, indicating that the two-state model is capable of explaining the variation in conformational parameters (h and λ^{-1}) for ATBC with the kind of solvent in a unified fashion. Using the previously estimated f_R of 0.55 ± 0.03 [5] along with the f_{1698} values, we find that F_R's in 2PrOH and 2BuOH are 0.53 ± 0.03 and 0.75 ± 0.04, respectively.

It follows from eqs. 3 and 4 that h^{-1} should vary linearly with λ according to the relation

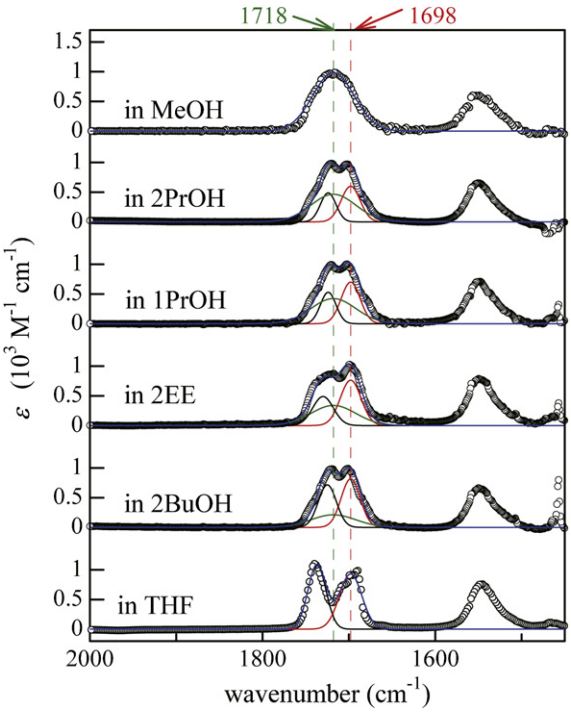

Fig. 8. IR spectra (molar absorption coefficient ϵ vs wavenumber) for ATBC460K in 2PrOH at 35 °C, in 1PrOH at 40 °C, in 2EE at 25 °C, and in 2BuOH at 45 °C along with previous data [5] in THF and MeOH.

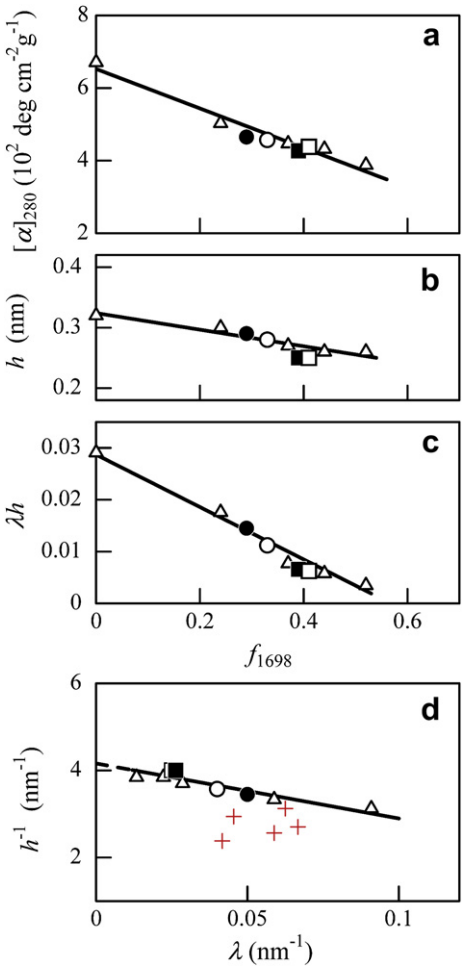

Fig. 9. Plots of $[\alpha]_{280}$ vs f_{1698} (a), h vs f_{1698} (b), λh vs f_{1698} (c), and h^{-1} vs λ (d) for ATBC in 2PrOH at 35 °C (filled circles), in 1PrOH at 40 °C (open circles), in 2EE at 25 °C (filled squares), in 2BuOH at 45 °C (open squares), and in THF-MeOH mixtures at 25 °C (triangles) [5]. The crosses in (d) represent data for ATPC in various solvents at 25–33 °C [10,11].

$$h^{-1} - h_F^{-1} = -\frac{h_R^{-1} - h_F^{-1}}{\lambda_F - \lambda_R}(\lambda - \lambda_F) \quad (5)$$

The panel d of Fig. 9 shows this to be well born out, indicating that the increases in flexibility and helix pitch are closely correlated to each other through the breaking of intramolecular H-bonds. On the other hand, virtually no such correlation between h and λ^{-1} can be observed for ATPC whose data in various solvents are shown by crosses in this panel. Thus, the two-state model is inapplicable to this amylose derivative in various solvents. This contrast may be explained by the finding [11] that both helix extension and stiffening of ATPC are affected primarily by the bulkiness of solvent molecules (ketones or esters).

4. Concluding remarks

The number fraction f_{1698} of intramolecular H-bonds in ATBC significantly decreases with the order of THF > 2BuOH ~ 2EE > 1PrOH > 2PrOH > MeOH, which is consistent with the decreasing order of dielectric constant, while the contour length h per residue increases and the Kuhn segment length λ^{-1} decreases in almost the same solvent order. The relation among h, λ^{-1}, and f_{1698} is successfully explained by a two-state model consisting of random sequences of rigid and loose helices, as is the case in THF-MeOH mixtures [5]. The increase in helix pitch stems primarily from the breaking of intramolecular H-bonds between the C=O and NH groups of ATBC, differing from the ATPC case in which the helix extension may be considered as due to the wedging of solvent molecules (ketones and esters) into the domain sandwiched between the neighboring phenylcarbamate groups [11]. In other words, the difference in the bulkiness between butyl and phenyl groups plays an important role in polymer–solvent interactions. This difference may have something to do with the experimental fact that amylose alkyl (methyl and isopropyl) carbamates are not useful as a chiral stationary phase in contrast to amylose phenyl carbamates [22,23].

Although the theta state is seldom found for stiff polymers [24], 2PrOH and 1PrOH at 35 °C are theta solvents for ATBC as is the case with ethyl acetate and methyl acetate for ATPC. The presence of theta solvents may also be a feature of amylose carbamates whose crystal structure has not as yet been reported probably because of difficulty in crystallization.

Acknowledgments

The authors thank Prof. Takahiro Sato (Osaka Univ.) for valuable discussions. The synchrotron radiation experiments were performed at the BL40B2 in SPring-8 with the approval of the Japan Synchrotron Radiation Research Institute (JASRI) (Proposal #2007A1034, #2007B1296, and #2008A1313).

References

[1] Alberts B, Johnson A, Lewis J, Raff M, Roberts K, Walter P. Molecular biology of the cell. 4th ed. New York: Garland Science; 2002.
[2] Gellman SH. Acc Chem Res 1998;31:173–80.
[3] Hill DJ, Mio MJ, Prince RB, Hughes TS, Moore JS. Chem Rev 2001;101:3893–4011.
[4] Schurig V, Zhu J, Muschalek V. Chromatographia 1993;35:237–40.
[5] Terao K, Murashima M, Sano Y, Arakawa S, Kitamura S, Norisuye T. Macromolecules 2010;43:1061–8.
[6] Kratky O, Porod G. Recl Trav Chim Pays-Bas 1949;68:1106–22.
[7] Zugenmaier P, Steinmeier H. Polymer 1986;27:1601–8.
[8] Yamakawa H. Helical wormlike chains in polymer solutions. Berlin: Springer; 1997.
[9] Yamakawa H. Polym J 1999;31:109–19.
[10] Terao K, Fujii T, Tsuda M, Kitamura S, Norisuye T. Polym J 2009;41:201–7.
[11] Fujii T, Terao K, Tsuda M, Kitamura S, Norisuye T. Biopolymers 2009;91:729–36.
[12] Kitamura S, Yunokawa H, Mitsuie S, Kuge T. Polym J 1982;14:93–9.
[13] Zimm BH. J Chem Phys 1948;16:1099–116.
[14] Berry GC. J Chem Phys 1966;44:4550–64.
[15] Holtzer AJ. J Polym Sci 1955;17:432–4.
[16] Nakamura Y, Norisuye T. J Polym Sci Part B Polym Phys 2004;42:1398–407.
[17] Benoit H, Doty P. J Phys Chem 1953;57:958–63.
[18] Konishi T, Yoshizaki T, Saito T, Einaga Y, Yamakawa H. Macromolecules 1990;23:290–7.
[19] Yamakawa H, Fujii M. Macromolecules 1974;7:128–35.
[20] Yamakawa H, Yoshizaki T. Macromolecules 1980;13:633–43.
[21] Chisaka S, Norisuye T. J Polym Sci Part B Polym Phys 2001;39:2071–80.
[22] Yamamoto C, Okamoto Y. Bull Chem Soc Jpn 2004;77:227–57.
[23] Okamoto Y, Kawashima M, Hatada K. J Am Chem Soc 1984;106:5357–9.
[24] Norisuye T. Prog Polym Sci 1993;18:543–84.